Adsorption (2015) 21:479–488
DOI 10.1007/s10450-015-9685-5

Activated carbon fibers for efficient VOC removal from diluted streams: the role of surface morphology

Guillaume B. Baur[1] · Igor Yuranov[1] · Albert Renken[1] · Lioubov Kiwi-Minsker[1,2]

Received: 9 April 2015 / Revised: 26 June 2015 / Accepted: 27 June 2015 / Published online: 16 July 2015

Abstract The effect of the micropore structure of activated carbon fibers (ACFs) on the adsorption of toluene at low concentration (10–80 ppmv) was studied over two types of ACFs. Both adsorbents presented similar surface chemistry but different porous structure: one ACF was ultramicroporous ($d_{pore} < 1$ nm) and the other supermicroporous ($d_{pore} \sim 1$ to 2 nm). Toluene adsorption isotherms were determined for both ACFs and were found to be consistent with Dubinin–Radushkevich (D–R) model. The toluene adsorption enthalpies calculated from temperature-programmed desorption profiles at temperatures below 330 K were close to the values obtained from D–R equations. Larger adsorption strength was found in the ultramicroporous adsorbent as compared to the supermicroporous one suggesting that the pore shape strongly influences the adsorption mechanism. The adsorbent with a lower specific surface area but narrower micropores could be more efficient at high temperatures than an adsorbent with large pore volume and wider micropores. The findings reported have a big importance for correct choice of material when designing efficient structured adsorbing bed.

Keywords Activated carbon fibers · Microporosity · Adsorption · Volatile organic compounds

✉ Lioubov Kiwi-Minsker
lioubov.kiwi-minsker@epfl.ch

[1] Group of Catalytic Reaction Engineering, Ecole Polytechnique Fédérale de Lausanne, EPFL-SB-ISIC-GGRC, Station 6, 1015 Lausanne, Switzerland

[2] Tver Technical University, Tver, Russia 170026

1 Introduction

The removal of volatile organic compounds (VOC) received great attention during the last decades (Cal et al. 1997; Lillo-Rodenas et al. 2005; Dimotakis et al. 1995; Lillo-Rodenas et al. 2006) since the presence of these pollutants in the atmosphere even at low concentrations is detrimental for both human health and environment (Tancrede et al. 1987). Different sources of emissions were identified with industrial off-gases as the major anthropogenic one (Piccot et al. 1992).

The abatement of diluted VOC by adsorption was successfully reported several times (Foster et al. 1992; Popescu et al. 2003; El-Sayed and Bandosz 2001). This method allows complete VOC removal with minimal energy input. The adsorbent of choice is often activated carbon due to its versatility towards different compounds (Hayashi et al. 2005). Moreover, its adsorption capacity is often higher as compared to other adsorbents such as zeolites or polymers due to its very high porosity (Mangun et al. 1998). Activated carbon can be used as adsorbent in several forms like granules, pellets, powders or fibers. Among them, activated carbon fibers (ACFs) consisting of microfilaments with high specific surface area, present smaller mass transfer limitations and lower pressure drop as compared to the other types of activated carbon (Singh et al. 2002; Das et al. 2004).

Numerous publications are devoted to VOC abatement by activated carbon (Lillo-Rodenas et al. 2011; Foster et al. 1992; Mangun et al. 2001; Baur et al. 2015b) reporting their adsorption capacity. However, the adsorption thermodynamic data are often missing limiting an understanding of the adsorbent-adsorbate interactions. The knowledge of the adsorption thermodynamic data are also crucial for the design of an efficient adsorbent bed. It allows forecasting its life time before regeneration.

In our previous work (Baur et al. 2015a) the effect of the ACFs surface chemistry on toluene and acetaldehyde removal was reported. The results showed that the presence of surface O-containing groups decreases the adsorption capacity towards toluene but increases for acetaldehyde. A systematic study of the same ACFs with different O-content highlighted the importance of this parameter for the adsorption capacity.

The present study investigates the effect of microporosity on toluene adsorption at low concentration (<100 ppmv) over two commercial ACFs. The adsorption isotherms were obtained at different temperatures (298–353 K) by varying toluene partial pressure (1–8 Pa). The experimental results were compared to Langmuir (1918), Dubinin–Radushkevich (D–R) (Dubinin 1960) and Dubinin–Astakhov (D–A) (Dubinin and Stoeckli 1980) adsorption models by varying model parameters to fit the experimental data. The Langmuir model assumes monolayer coverage of the adsorbent whereas the D–R and the D–A equations are a semi-empirical model based on the 'pore filling mechanism' (Dubinin 1967). This study analyses the differences in the adsorption thermodynamics for two microporous adsorbents in the low VOC concentration range. The adsorption enthalpy has been determined by modelling the adsorption isotherms and temperature-programmed desorption (TPD) of toluene for both adsorbents. The adsorption enthalpy values determined by both methods were then compared.

2 Experimental part

2.1 Material

ACFs were purchased from by Kynol Europa GmbH (Hamburg, Germany). They are produced from Kynol novoloid (phenolic) precursor fibers by a one-step process combining both carbonization and chemical activation. Two types of the fibers were used, namely: ACF-1 (SSA $\sim$1000 m^2 g^{-1}) and ACF-2 (SSA $\sim$2000 m^2 g^{-1}). Prior to adsorption measurements the samples were heated at 673 K during 30 min.

The toluene was purchased from VWR (99.9 % VWR Chemicals, AnalaR NORMAPUR). Argon, CO_2 and helium (99.999 %) were provided by Carbagas.

The ACFs characterization techniques, scanning electron microscopy (SEM), porosity determination via N_2 isotherms and surface chemistry analysis are presented elsewhere (Baur et al. 2015a). The microporosity characterization via CO_2 isotherms was carried out in a Micromeretics Baseflex Surface Characterization unit at subatmospheric pressures.

2.2 Dynamic adsorption measurements

Toluene adsorption isotherms on the ACF-1 and ACF-2 were obtained by measuring the adsorption capacity at different temperatures and toluene partial pressures. The experimental setup used for adsorption experiments was recently presented in details (Baur et al. 2015a). ACF samples (10 $\pm$ 0.1 mg) were outgassed in a He flow (40 cm^3 min^{-1}) at 673 K. The desired adsorption temperature was then set and kept constant during the experiment (298–353 K). The toluene concentrations (10–80 ppmv) were set through a gas generator. The total gas flow was 300 cm^3 min^{-1} STP. Toluene is passing through the adsorbent bed until its saturation. The inert tracer signal (Ar 2 % v/v in He) was obtained independently. In such a manner a toluene breakthrough curve is obtained. The adsorption capacity is calculated by numerical integration of the area defined by the breakthrough curve and Argon signal. Other experiment details are available elsewhere (Baur et al. 2015a).

2.3 Temperature-programmed desorption (TPD)

TPD experiments were carried out in the same setup used for toluene adsorption. Prior to desorption experiment ACF samples (10 $\pm$ 0.1 mg) were saturated by toluene at 298 K before being heated in a He flow (100 cm^3 min^{-1}) at different temperature ramps (3–30 K min^{-1}). The outlet concentration of desorbed toluene was continuously monitored by a mass spectrometer (Hiden Analytical HPR 20 QIC) and plotted as a function of temperature. Numerical integration of the toluene desorption peak was carried out to calculate the adsorption–desorption mass balance. In all cases the mass balance was larger than 95 %.

3 Results and discussion

3.1 Characterization of ACFs adsorbents

The characterization of ACF-1 and ACF-2 were carried out using scanning electron microscopy, N_2 physisorption at 77 K (specific surface area and porosity) and TPD. SEM gives a general view of the elementary filaments constituting the ACFs. The porosity analysis of ACF-1 and ACF-2 revealed two microporous adsorbents exhibiting a type I isotherm according to the IUPAC classification. A deeper analysis of the nitrogen isotherms of both adsorbent showed that ACF-1 is ultramicroporous (pore diameter <1 nm) whereas ACF-2 has supermicropores (1–2 nm) (Baur et al. 2015a).

More careful characterization of the microporosity of the ACF adsorbents was obtained via CO_2 adsorption at

subatmospheric pressures (Cazorla-Amoros et al. 1998). Such technique is known as a complementary method to N_2 adsorption isotherms. It allows assessing the narrow microporosity where N_2 adsorption can be kinetically restricted (Garrido et al. 1987). The volume of narrow microporosity was calculated applying the Dubinin–Radushkevish equation to the CO_2 adsorption isotherms at 273 K (Cazorla-Amoros et al. 1996). The narrow micropore volume is presented in Table 1. As can be seen, for ACF-1 the volume of narrow microporosity calculated with the CO_2 isotherm is similar to the total micropore volume calculated with N_2 isotherms indicating that the major part of the micropores has diameter smaller than 1 nm. On the opposite, the narrow micropore volume of ACF-2 represents only a third of its total pore volume, the remaining part being larger micropores. Hence, this analysis confirms the conclusions obtained from N_2 adsorption isotherms (Baur et al. 2015a). ACF-1 is an ultramicroporous adsorbent whereas ACF-2 shows mostly supermicroporosity.

The surface chemistry analysis was addressed via temperature programmed desorption revealing the presence of O-containing groups in low quantities on the surface of both ACFs (Baur et al. 2015a). It was reported that O-containing groups reduce the carbon adsorption capacity of toluene at constant porosity (Lillo-Rodenas et al. 2005). To obtain similar surface chemistry of both ACFs samples a heat treatment under inert (He) at 673 K to remove part of the O-containing groups was performed. The TPD patterns of ACF-1 and ACF-2 after and before pretreatment at 673 K are shown in Fig. 1. As can be seen the low temperature CO_2 peaks (600 K) attributed to the decomposition of carboxylic groups do not appear on pretreated fibers indicating a removal of the latter upon heat treatment. The lactones, lactol and anhydride groups characterized by the shoulder at 800 K remain on the fibers (Figueiredo et al. 1999). The O-containing groups desorbing as CO at higher temperature such as carbonyl and phenol are also remaining on the surface after pretreatment.

The characteristics of ACF-1 and ACF-2 pretreated at 673 K are summarized in Table 1. ACF-1 shows lower specific area and smaller average pore diameter as compared to ACF-2. Despite the difference in surface area, the oxygen content between ACF-1 and ACF-2 after heat treatment is extremely low for both fibers. Therefore, it was assumed that the polarity created by the surface oxygen group was negligible and should not influence the toluene adsorption capacity. Thus, the microporosity is suggested to be the only difference between ACF-1 and ACF-2 and the influence of pore diameter on toluene adsorption can be studied.

3.2 Toluene adsorption isotherm

Toluene adsorption typical results are shown in Fig. 2 as breakthrough curves. The adsorption capacity of the ACFs materials was determined by a numerical integration of the area between the toluene concentration curve and the argon curve. All the adsorption capacities presented in this paper

Table 1 Characteristics of ACFs

Sample	SSA_{BET} (m^2 g^{-1})	Pore volume (N_2) (cm^3 g^{-1})	Pore volume (CO_2) (cm^3 g^{-1})	Pore diameter (nm)	Oxygen content (μmol g^{-1})
ACF-1	1030 ± 50	0.40 ± 0.02	0.38 ± 0.01	<1	500 ± 50
ACF-2	2220 ± 50	0.95 ± 0.02	0.34 ± 0.01	1–2	370 ± 50

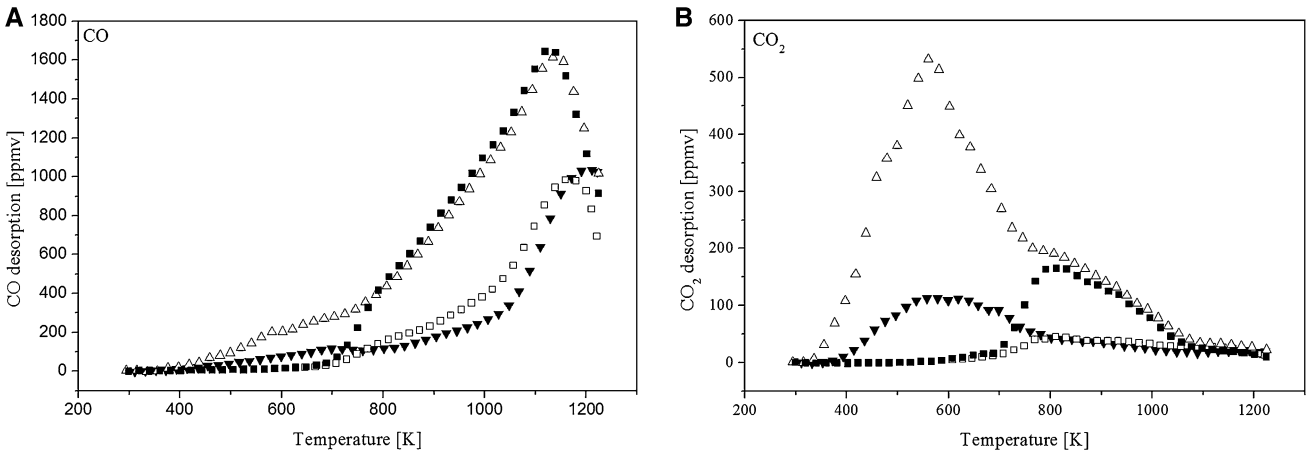

Fig. 1 TPD profiles of original ACF-1 (*white up-pointing triangle*), original ACF-2 (*black down-pointing triangle*), pretreated ACF-1 (*black square*) and preteated ACF-2 (*white square*) (10 K min^{-1}, 50 cm^3 min^{-1})

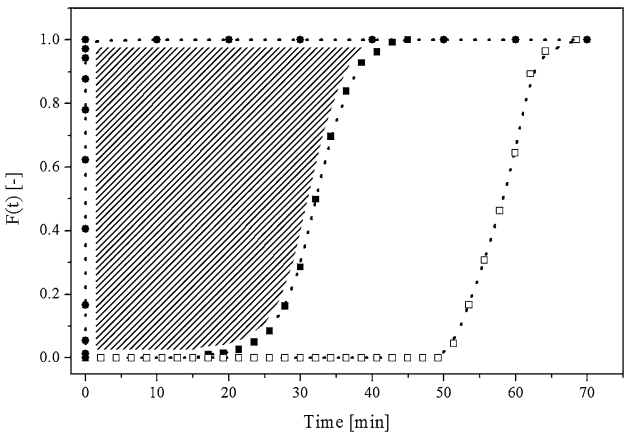

Fig. 2 Toluene (80 ppmv) breakthrough curves for ACF-1 (*black square*) and ACF-2 (*white square*) and Argon 2 % (v/v) tracer (*black circle*) at 298 K

were obtained similarly to Fig. 2. In all the adsorption experiments the outlet toluene concentration was zero signifying a total toluene removal until the breakthrough.

As can be seen in Fig. 2 the adsorption capacity of ACF-2 is larger than ACF-1. This result can be explained by the larger specific surface area and pore volume of ACF-2 (Table 1). By varying the toluene concentration (10–80 ppmv or 1–8 Pa) and temperature of adsorption (298–353 K) a set of adsorption isotherms was obtained for both ACFs (Fig. 3). Langmuir and van't Hoff Eqs. (1, 2) were first used to fit the experimental data.

$$q = q_{\max,L}\frac{KP_{toluene}}{1 + KP_{toluene}} \quad (1)$$

where

$$K = K_0 \exp\left(\frac{-\Delta H^0_{ads}}{RT}\right) \quad (2)$$

Table 2 Langmuir model parameters for toluene adsorption (298 K)

Adsorbent	$q_{\max,L}$ (mol kg^{-1})	K_0 (Pa^{-1})	ΔH^0_{ads} (kJ mol^{-1})
ACF-1	2.9 ± 0.5	4.3 ± 0.3·10^{-4}	−24.4 ± 4.2
ACF-2	4.6 ± 2	1.3 ± 0.1·10^{-2}	−11.8 ± 4.2

The model variables were the total monolayer surface coverage as defined by the Langmuir model $(q_{\max,L})$, pre-exponential factor of the adsorption equilibrium constant (K_0) and adsorption enthalpy (ΔH^0_{ads}).

Langmuir model assumes that maximum adsorbed concentration $(q_{\max,L})$ is not a function of the adsorption temperature and the lateral interactions are negligible implying that the adsorption enthalpy does not depend on the surface coverage. The fitted model parameters obtained for the studied adsorbents are presented in Table 2.

As shown in Fig. 3 the Langmuir model fits well the experimental data of toluene adsorption on ACFs. The supermicroporous ACF-2 has higher maximum toluene adsorption capacity ($q_{max,L}$) at 298 K as compared to ACF-1 due to the larger specific surface area of the ACF-2 (Table 1).

The adsorption enthalpy values obtained for both ACFs are too low and even smaller than the heat of condensation (−38 kJ mol^{-1}) (Pitzer and Scott 1943). Since this result is meaningless, we concluded that Langmuir model is not suitable to describe the toluene adsorption on ACFs. The monolayer adsorption and the absence of lateral interactions are apparently not correct assumptions for microporous materials even at very low toluene partial pressure. Therefore, we assume that even in the 10–80 ppmv pressure range, a multilayer adsorption or a pore filling occurs suggesting another adsorption model.

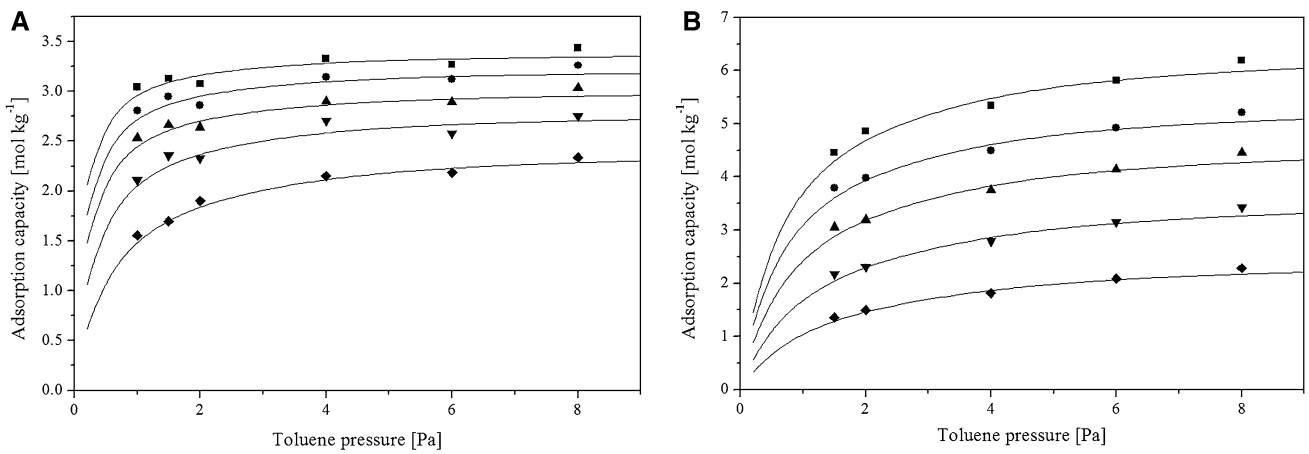

Fig. 3 Toluene adsorption isotherms on ACF-1 (**a**) and ACF-2 (**b**) fitted with the Langmuir model at: 298 K (*black square*), 308 K (*black circle*), 318 K (*black up-pointing triangle*), 333 K (*black down-pointing triangle*), 353 K (*black diamond*)

The Dubinin–Radushkevich (D–R) model (Eq. 3) was originally developed for benzene adsorption on activated carbon (Dubinin 1989).

$$W = W_0 \exp\left(-\left(\frac{A}{\beta E_0}\right)^2\right) \tag{3}$$

This semi-empirical equation was developed for sub-critical vapors in microporous solids where the adsorption process follows a pore filling mechanism. A liquid-like adsorbed phase in the micropores is assumed. Vapors adsorption on many microporous solids, such as activated carbon or zeolites, can be described by the D–R equation. A particular characteristic of the D–R model is the temperature independence of the characteristic adsorption energy (E_0). It implies that adsorption data obtained at one temperature allow determining the characteristic adsorption energy. The model variables are the maximum adsorbed volume (W_0) and the characteristic adsorption energy (E_0). The parameter β is a constant depending on the nature of the adsorbate. In the case of toluene β is 1.28 (Wu et al. 2002).

The parameter A represents the Polyani adsorption potential. The value of A is equal to the difference between the chemical potential of the adsorbate in the liquid state and in the adsorbed state at the same temperature.

$$A = RT \ln\left(\frac{p_0}{p}\right) \tag{4}$$

p_0 is the vapor pressure, p is the adsorbate partial pressure and T is the temperature at which the adsorption experiment took place. In this model the adsorbed phase is supposed to be liquid. Therefore, the saturation adsorption capacity corresponds to the maximum adsorbed liquid volume in the microporous network.

$$q_{\max} = W_0 / v_M \tag{5}$$

where W_0 is the maximum adsorbed volume and v_M is the liquid molar volume (toluene = 106.3 ml mol^{-1}). This is opposite to Langmuir model where the maximum adsorption capacity is equal to monolayer coverage of the adsorbent surface.

The saturation capacity is temperature dependent since the liquid molar volume is a function of temperature. The integral form of the temperature dependence of the saturation adsorption capacity is:

$$q_{\max} = q_{\max,0} \exp(-\delta(T - T_0)) \tag{6}$$

where $q_{\max,0}$ is the saturation adsorption capacity at a reference temperature T_0 (298 K) and δ is the thermal expansion coefficient of the saturation concentration. For toluene δ is 0.001 K^{-1} (Duong 1998).

The adsorption enthalpy of the D–R model can be calculated from the van't Hoff equation

$$\frac{\Delta H}{RT^2} = -\left(\frac{\partial \ln p}{\partial T}\right)_q \tag{7}$$

By taking the total derivative of the D–R equation (Eq. 3), the Clausius-Clapeyron equation and substituting them in Eq. 7, the expression of the isosteric heat is obtained for a constant loading:

$$-\Delta H = RT \ln\left(\frac{p_0}{p}\right) + \Delta H_{vap} + \frac{(\beta E_0)^2 \delta T}{2RT \ln\left(\frac{p_0}{p}\right)} \tag{8}$$

where ΔH_{vap} is the heat of condensation. For toluene −38 kJ mol^{-1} is used.

The isosteric adsorption enthalpy is the summation of three terms: the first represents the adsorption potential, the second is the heat of vaporization and the third expresses the influence of the maximum capacity variation with temperature. For the sake of clarity the isosteric adsorption enthalpy is expressed in terms of fractional loading:

$$-\Delta H = \Delta H_{vap} + \beta E_0 \left(\ln\left(\frac{1}{\theta}\right)\right)^{1/2} + \frac{\beta E_0 \delta T}{2}\left(\ln\left(\frac{1}{\theta}\right)\right)^{-1/2} \tag{9}$$

with

$$\theta = \frac{q}{q_{\max}} \tag{10}$$

Following Eq. 9, the adsorption enthalpy is by definition larger than the heat of vaporization and depends on the characteristic adsorption energy (E_0) and on the adsorbent fractional loading (θ). The maximum adsorption capacity and the characteristic adsorption energy were obtained by fitting the experimental data to Eq. 3 for all the isotherms and both adsorbents (Fig. 4).

The D–R model fits well the experimental data for ACF-2. The curve determination coefficients (R^2) was found to be larger than 0.98 proving the validity of the model used. Pore filling mechanism seems to be a suitable model for toluene adsorption on ACF-2. For ACF-1 the R^2 is slightly lower (0.85) but remains acceptable. The parameters (E_0 and $q_{\max,0}$) obtained are presented in Table 3. D–R model predicts a higher maximum toluene adsorption capacity (q_{max}) at 298 K of ACF-2 (9.6 mol kg^{-1}) as compared to ACF-1 (4 mol kg^{-1}) according to its larger pore volume (Table 1). The thermodynamic adsorption parameter (E_0) also indicates a difference in toluene adsorption mechanism on both ACFs samples. The characteristic adsorption energy (E_0) is 28 ± 6 and 17 ± 2 kJ mol^{-1} for ACF-1 and ACF-2, respectively. High characteristic adsorption energy

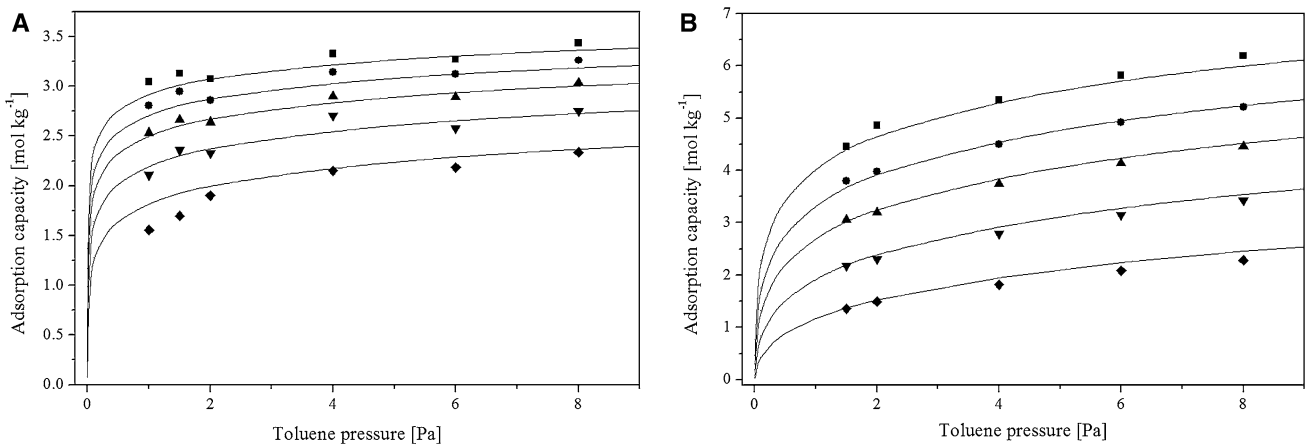

Fig. 4 Toluene adsorption isotherms on ACF-1 (**a**) and ACF-2 (**b**) fitted with the D–R model at: 298 K (*black square*), 308 K (*black circle*), 318 K (*black up-pointing triangle*), 333 K (*black down-pointing triangle*), 353 K (*black diamond*)

Table 3 Toluene adsorption parameters (298 K)

Adsorbent	Dubinin–Radushkevich model			Dubinin–Astakhov model		
	$q_{max,0}$ (mol kg^{-1})	n	E_0 (kJ mol^{-1})	$q_{max,0}$ (mol kg^{-1})	n	E_0 (kJ mol^{-1})
ACF-1	4 ± 0.4	2	28 ± 6	3.6 ± 0.3	3	27 ± 7
ACF-2	9.6 ± 1.5	2	17 ± 2	9.5 ± 1.5	1.9	17 ± 2

suggests stronger adsorbate–adsorbent interactions. It is then concluded that adsorbents with ultramicropores have stronger interactions with the adsorbate.

The fitting obtained by the D–R model for both adsorbent in Fig. 4 could be further improved by using the Dubinin–Astakhov (D–A) model (Dubinin and Stoeckli 1980). This model is also based on the Polyani adsorption potential and the characteristic adsorption energy and only differs from the D–R equation by the exponent (n):

$$W = W_0 \exp\left(-\left(\frac{A}{\beta E_0}\right)^n\right) \quad (11)$$

In the D–R model the exponent is $n = 2$ whereas it can take a random value in the D–A model. This exponent represents the adsorbent surface heterogeneity and is linked to the sharpness of the pore size distribution being specific for each particular adsorbent (Terzyk et al. 2002). For non-homogeneous pore size distribution the typical values are found between 1 and 2, whereas it increases for narrower pore size distribution (Dubinin 1989). Molecular sieving carbon, for example, has a heterogeneity parameter of 3 and for crystalline zeolite this parameter can increase up to 6 (Hutson and Yang 1997).

The D–A model was used herein to fit the experimental data of toluene adsorption on both ACFs. The characteristic adsorption energy (E_0), the saturation capacity ($q_{max,0}$) and the surface heterogeneity (n) were adjusted. The results are presented in Fig. 5.

Similarly to the D–R model, the D–A model shows a good fitting of the experimental data. For ACF-2 the optimized parameters were extremely close to the D–R ones. The heterogeneity parameter was close to 2, the characteristic adsorption energy was 17 ± 2 kJ mol^{-1} and the saturation capacity was 9.5 ± 1.5 mol kg^{-1}, being in accordance with the D–R model. For ACF-1 the D–A model gave improved fitting with $n = 3$. The curve determination coefficient was slightly increased with the D–A model, particularly for the isotherm at 353 K ($R^2 = 0.91$ instead of 0.85). However due to the high degree of freedom during the linearization, the error on the parameters is relatively important for the D–A model. It is then not possible to insure that the D–A model is more suitable for ACF-1 despite the better fitting. Hence the parameter values found with the D–R model will be used. The parameters of the D–R and the D–A equation are summarized in Table 3.

To further prove the validity of the D–R model, the isosteric adsorption enthalpy was evaluated with Eq. 9 for 298 K and is presented as a function of fractional loading in Fig. 6. The dependency of the isosteric adsorption enthalpy on temperature was found to be negligible (0–3 kJ mol^{-1}) in the studied temperature range (298–353 K).

Figure 6 shows a decrease of the isosteric adsorption enthalpy with the coverage. The D–R model predicts a very high adsorption enthalpy for low loading, going to infinite at zero loading. The isosteric adsorption enthalpy decreases

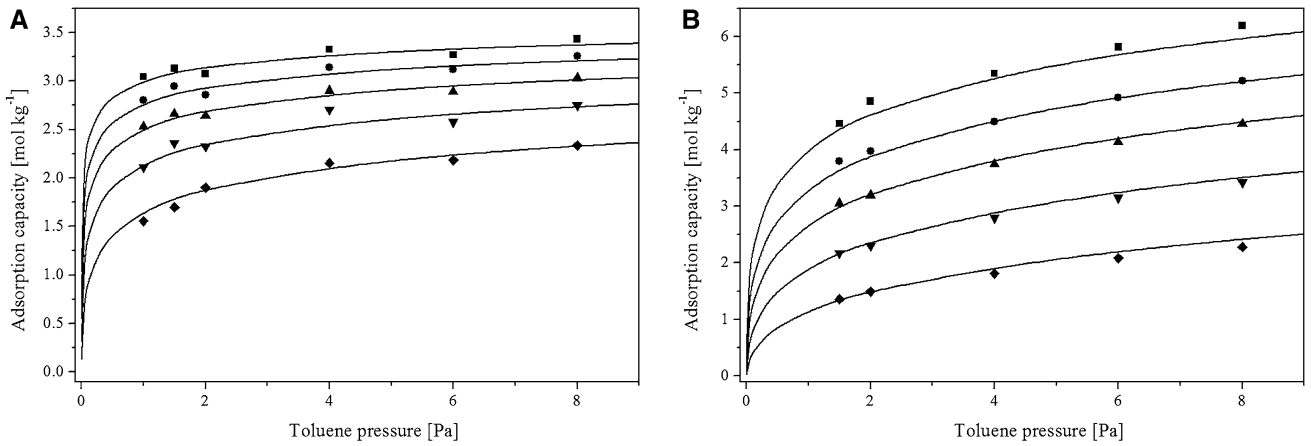

Fig. 5 Toluene adsorption isotherms on ACF-1 (**a**) and ACF-2 (**b**) fitted with the D–A model at: 298 K (*black square*), 308 K (*black circle*), 318 K (*black up-pointing triangle*), 333 K (*black down-pointing triangle*), 353 K (*black diamond*)

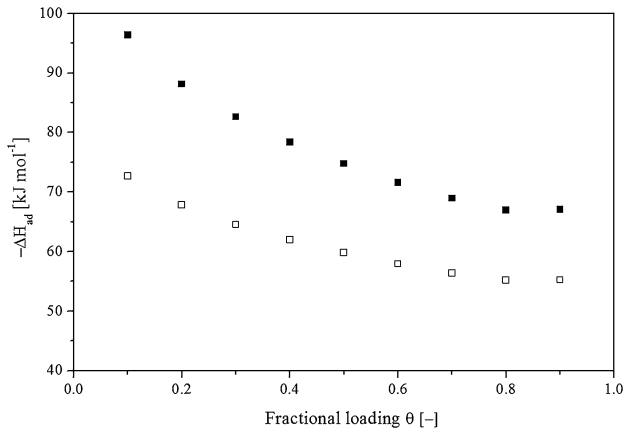

Fig. 6 Adsorption enthalpy in function of toluene fractional loading: ACF-1 (*black square*) and ACF-2 (*white square*)

with the fractional loading until a minimum whereas at fractional loading >0.95, it increases again (due to the thermal expansion coefficient of the saturation concentration in the third them of Eq. 9). In summary, the model is against any physical meaning at a fractional loading of 0 and 1. Therefore, the toluene adsorption in the range of 0.1–0.9 fractional loadings was studied.

The higher isosteric adsorption enthalpy calculated for ACF-1 (70–90 kJ mol^{-1}) as compared to ACF-2 (55–75 kJ mol^{-1}) is directly linked to their difference in characteristic adsorption energy (E_0). Toluene is therefore more strongly adsorbed in the pores of ACF-1.

The adsorption capacity at 298 K and 80 ppmv of toluene (8 Pa) were 31.6 and 57.0 wt% for ACF-1 and ACF-2, respectively, whereas their specific surface area are 1030 and 2220 $m^2\ g^{-1}$ (Table 1). The surface normalized adsorption capacity is then higher for ACF-1 (3.3×10^{-6} mol m^{-2}) as compared to ACF-2 (2.8×10^{-6} mol m^{-2}). Since the characterization revealed similar surface chemistry (O-containing groups), the larger normalized adsorption capacity for ACF-1 is explained by the porosity. Indeed, narrower pores were measured for ACF-1. The higher adsorption efficiency of ACF-1 is due to its ultramicroporosity (pore diameter <1 nm) as compared to supermicropores (pore diameter 1–2 nm) of ACF-2.

The influence of the micropore size on the VOC adsorption capacity of ACFs has been already studied (Foster et al. 1992; Mangun et al. 1998). For some adsorbates (ethane, propane, butane and pentane), a microporous adsorbent with a lower SSA can have a higher adsorption capacity due to narrower pores (Mangun et al. 1998). This phenomenon is called cross-over regime, meaning a higher adsorption capacity for a lower specific surface area. The pore filling in ultramicroporous adsorbents is enhanced and the available pore volume is used more efficiently as compared to supermicroporous one due to the higher overlap potential between the pore walls. In the present study, this phenomenon is observed for toluene adsorption. In the range of concentrations (10–80 ppmv), the degree of filling of ACF-1 ultramicropores is larger than ACF-2 supermicropores. Their fractional loading at 298 K and 8 Pa is 0.86 and 0.63, respectively. The lower specific surface area and smaller pore volume of ACF-1 is compensated by a more favorable pore shape leading to a larger toluene adsorption capacity under certain conditions. Thus, the adsorbent pore size along with specific surface area plays a crucial role in toluene removal by adsorption from highly diluted streams.

The narrower pore size of ACF-1 explains its larger adsorption enthalpy because of the stronger interactions of the pore walls. Such phenomenon can lead to a larger adsorption capacity of ACF-1, particularly at high temperature. For example at 353 K despite its lower specific surface area (Fig. 4a, b) the adsorption capacity of ACF-1

is larger as compared to ACF-2. A larger adsorption enthalpy is particularly interesting at high adsorption temperature. An adsorbent with a lower specific surface area but narrower micropores could be more efficient than an adsorbent with large pore volume and wider micropores. This phenomenon was already reported for low boiling point VOC (Mangun et al. 1998).

3.3 Temperature programmed desorption of toluene

Toluene desorption from the ACFs was carried using different temperature ramps. The TPD profiles recorded for the ACF-2 are plotted on Fig. 7

As shown can be seen, the desorption peak maximum shifts to higher temperatures with the temperature ramp. In order to determine the kinetic parameters (E_d, k) of desorption, TPD curves were numerically simulated. The simulations were carried out for five temperature ramps. By solving the mass balance and linear temperature variation simultaneously, TPD profiles can be simulated. The fitting to the experimental points is then adjusted by varying E_d and k. The mass balance is expressed as following:

$$F_{tot,0} \cdot y_{tol,0} - F_{tot} \cdot y_{tol} = R_d \cdot m_{ads} \tag{12}$$

where F_{tot} is the molar flow, y_{tol} the molar fraction of toluene and R_d the desorption rate. The inlet molar fraction ($y_{tol,0}$) is equal to 0 since the TPD experiment is carried out in He. Toluene desorption is then expressed as a function of the desorption rate constant (k_d):

$$-F_{tot} \cdot y_{tol} = -k_d \cdot Z_{tol}^m \cdot m_{ads} \tag{13}$$

where Z_{tol} is the concentration of adsorbed species and m the kinetic order of desorption. The rate constant of desorption can then be expressed with the activation energy of desorption.

$$n_{tol} = k_{d,0} \exp\left(\frac{-E_d}{R \cdot T}\right) \cdot Z_{tol}^m \cdot m_{ads} \tag{14}$$

The following differential equation was then obtained:

$$\frac{dZ_{tol}}{dt} = k_{d,0} \exp\left(\frac{-E_d}{R \cdot T}\right) \cdot Z_{tol}^m \tag{15}$$

The equation of the linear temperature increase is

$$T = T_0 + \gamma t; \quad \frac{dT}{dt} = \gamma \tag{16}$$

where T is temperature, T_0 the initial temperature, γ the temperature ramp and t the time. By combining Eqs. (15) and (16) and supposing a 1st order desorption kinetic:

$$\frac{dZ_{tol}}{dT} = \frac{k_{d,0}}{\gamma} \exp\left(\frac{-E_d}{R \cdot T}\right) \cdot Z_{tol} \tag{17}$$

The concentration of adsorbed species in function of temperature is then obtained. It depends on desorption rate and the activation energy of desorption. Supposing negligible activation energy of adsorption, the activation energy of desorption is approximated to the adsorption enthalpy (Cvetanović and Amenomiya 1967). Therefore, a comparison between the adsorption enthalpy obtained by the isotherm modelling and by TPD simulation could be performed.

As can be seen in Fig. 8 the simulation fits very well the experimental data suggesting that the toluene desorption from ACF-1 follows a 1st order kinetic. An apparent activation energy of desorption is found at 25 kJ mol^{-1}. This value is significantly lower than the adsorption enthalpy found with the isotherm modelling. Moreover, the simulated value is lower than the heat of condensation (−38 kJ mol^{-1}) being against physical meaning. Since ACF-1 presents a narrow microporosity (Table 1), it is supposed that mass transfer limitations may affect the

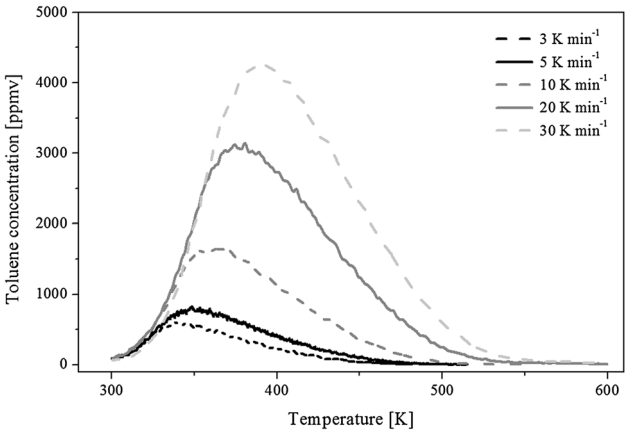

Fig. 7 TPD of toluene over ACF-2 (100 cm^3 min^{-1} in He) at different temperature ramps

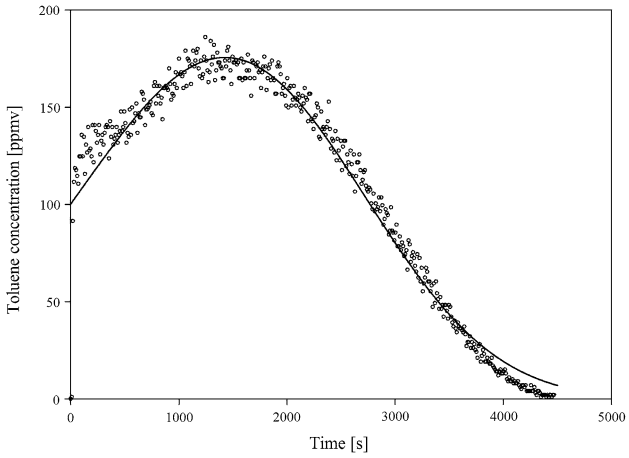

Fig. 8 TPD of toluene (experimental points and simulation line) over ACF-1 (3 K min^{-1}, 100 cm^3 min^{-1} in He)

desorption process explaining the low activation energy. Therefore, the activation energy of desorption obtained by simulation does not correspond to the adsorption enthalpy of toluene on ACF-1. It corresponds to a global constant that combines the adsorption enthalpy and a mass transfer coefficient. To overcome the effect of mass transfer and determine the adsorption enthalpy, only the lower temperature part of the TPD profile was used for simulations (Fig. 9). It is supposed that the mass transfer influence on the desorption rate is negligible at low temperature.

For ACF-1, due to its narrow microporosity, the simulation of the low temperature range of TPD profile did not give conclusive results since mass transfer limitations were not negligible even in the low temperature range. On the opposite, for ACF-2 a nice fitting was obtained by simulating only the first part of the desorption curve. As an example a TPD with the ramp of 3 K min^{-1} was chosen and is presented in Fig. 9. The influence of mass transfer on the rate of desorption encountered for ACF-1 does not appear with ACF-2 because of its wider micropores (Table 1). In the low temperature range, the desorption rate depends only on the activation energy of desorption. The adsorption enthalpy can then be obtained following the assumption that the activation energy of desorption is equal to the heat of desorption.

The simulation of the TPD profiles was performed for different temperature ramps (3–30 K min^{-1}) for the first

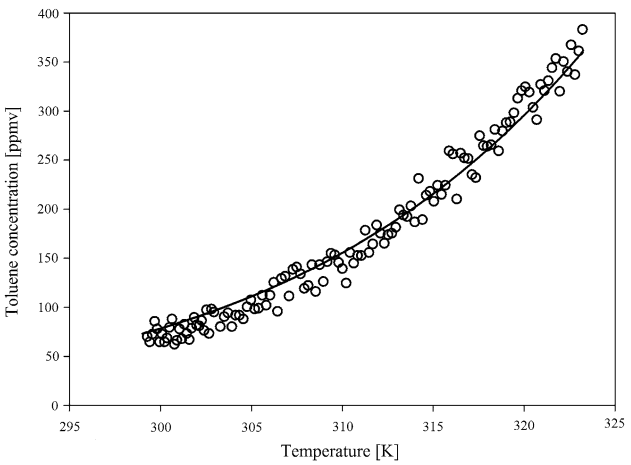

Fig. 9 Simulation of initial part of toluene TPD over ACF-2 (3 K min^{-1}, 100 cm^3 min^{-1} in He)

Table 4 Adsorption enthalpy determined through TPD and isotherm

Sample	ΔH^0_{ads} (kJ mol^{-1})	
	Isotherms	TPD
ACF-1	-67 ± 6	–
ACF-2	-57 ± 2	-53 ± 3

10 % of toluene desorption. The threshold limit of 10 % adsorbate desorption was arbitrary chosen assuming that the mass transfer does not influence the desorption rate and the coverage was supposed constant. With these assumptions, an initial activation energy of desorption of 53 kJ mol^{-1} was calculated. This value was identical for all the temperature ramps justifying the assumptions used. Moreover, as presented in Table 4 the adsorption enthalpy obtained for ACF-2 is very close the adsorption enthalpy calculated from the adsorption isotherms. The similarity between the adsorption enthalpy values determined by both TPD and isotherm methods confirm also suitable isotherm modelling. Pore filling mechanism suggested by the D–R and the D–A model is therefore likely to occur.

4 Conclusions

Adsorption of toluene was studied over two different samples: ACF-1 ultramicroporous ($d_{pore} < 1$ nm) and ACF-2 supermicroporous ($d_{pore} \sim 1$ to 2 nm) with similar surface chemistry characterized by the amount of O-containing groups. The effect porosity on the toluene adsorption capacity was addressed via analysis of the adsorption isotherms and TPD profiles. Dubinin–Radushkevich (D–R) model based on a pore filling mechanism described well the experimental adsorption isotherms. Based on this modelling the characteristic energy and the adsorption enthalpy were calculated for both ACFs revealing that the toluene is more strongly adsorbed in ultramicroporous ACF-1 as compared to supermicroporous ACF-2. Therefore, for practical applications especially at high adsorption temperature the ultramicroporous ACF-1 is the adsorbent of choice.

Toluene TPD experiments were carried out over both samples and successfully simulated in the low temperature (<330 K) range where mass-transfer limitations are absent. The adsorption enthalpy calculated from TPD results was close to the values determined from the D–R isotherm model.

Acknowledgments Research described in this article was supported by Philip Morris International.

References

Baur, G.B., Beswick, O., Spring, J., Yuranov, I., Kiwi-Minsker, L.: Activated carbon fibers for efficient VOC removal from diluted streams: the role of surface functionalities. Adsorption (2015a). doi:10.1007/s10450-015-9667-7

Baur, G.B., Yuranov, I., Kiwi-Minsker, L.: Activated carbon fibers modified by metal oxide as effective structured adsorbents for acetaldehyde. Catal. Today (2015b). doi:10.1016/j.cattod.2014.11.021

Cal, M.P., Rood, M.J., Larson, S.M.: Gas phase adsorption of volatile organic compounds and water vapor on activated carbon cloth. Energy Fuels **11**(2), 311–315 (1997)

Cazorla-Amoros, D., Alcaniz-Monge, J., de la Casa-Lillo, M.A., Linares-Solano, A.: CO_2 as an adsorptive to characterize carbon molecular sieves and activated carbons. Langmuir **14**(16), 4589–4596 (1998)

Cazorla-Amoros, D., Alcaniz-Monge, J., Linares-Solano, A.: Characterization of activated carbon fibers by CO_2 adsorption. Langmuir **12**(11), 2820–2824 (1996)

Cvetanović, R.J., Amenomiya, Y.: Application of a temperature-programmed desorption technique to catalyst studies. In: Eley, D.D., Pines, H., Paul, B.W. (eds.) Advances in Catalysis, vol. 17, pp. 103–149. Academic Press, New York (1967)

Das, D., Gaur, V., Verma, N.: Removal of volatile organic compound by activated carbon fiber. Carbon **42**(14), 2949–2962 (2004)

Dimotakis, E.D., Cal, M.P., Economy, J., Rood, M.J., Larson, S.M.: Chemically treated activated carbon cloths for removal of volatile organic carbons from gas streams—evidence for enhanced physical adsorption. Environ. Sci. Technol. **29**(7), 1876–1880 (1995)

Dubinin, M.M.: The potential theory of adsorption of gases and vapors for adsorbents with energetically nonuniform surfaces. Chem. Rev. **60**(2), 235–241 (1960)

Dubinin, M.M.: Adsorption in micropores. J. Colloid Interface Sci. **23**(4), 487–499 (1967)

Dubinin, M.M.: Fundamentals of the theory of adsorption in micropores of carbon adsorbents—characteristics of their adsorption properties and microporous structures. Carbon **27**(3), 457–467 (1989)

Dubinin, M.M., Stoeckli, H.F.: Homogeneous and heterogeneous micropore structures in carbonaceous adsorbents. J. Colloid Interface Sci. **75**(1), 34–42 (1980)

Duong, D.D.: Adsorption Analysis: Equilibria and Kinetics. Series on chemical engineering, vol. 2. Imperial College Press, London (1998)

El-Sayed, Y., Bandosz, T.J.: A study of acetaldehyde adsorption on activated carbons. J. Colloid Interface Sci. **242**(1), 44–51 (2001)

Figueiredo, J.L., Pereira, M.F.R., Freitas, M.M.A., Orfao, J.J.M.: Modification of the surface chemistry of activated carbons. Carbon **37**(9), 1379–1389 (1999)

Foster, K.L., Fuerman, R.G., Economy, J., Larson, S.M., Rood, M.J.: Adsorption characteristics of trace volatile organic-compounds in gas streams onto activated carbon-fibers. Chem. Mater. **4**(5), 1068–1073 (1992)

Garrido, J., Linaressolano, A., Martinmartinez, J.M., Molinasabio, M., Rodriguezreinoso, F., Torregrosa, R.: Use of N_2 vs Co_2 in the characterization of activated carbons. Langmuir **3**(1), 76–81 (1987)

Hayashi, T., Kumita, M., Otani, Y.: Removal of acetaldehyde vapor with impregnated activated carbons: effects of steric structure on impregnant and acidity. Environ. Sci. Technol. **39**(14), 5436–5441 (2005)

Hutson, N.D., Yang, R.T.: Theoretical basis for the Dubinin–Radushkevitch (D–R) adsorption isotherm equation. Adsorpt. J. Int. Adsorpt. Soc. **3**(3), 189–195 (1997)

Langmuir, I.: The adsorption of gases on plane surfaces of glass, mica and platinum. J. Am. Chem. Soc. **40**, 1361–1403 (1918)

Lillo-Rodenas, M.A., Cazorla-Amoros, D., Linares-Solano, A.: Behaviour of activated carbons with different pore size distributions and surface oxygen groups for benzene and toluene adsorption at low concentrations. Carbon **43**(8), 1758–1767 (2005)

Lillo-Rodenas, M.A., Cazorla-Amoros, D., Linares-Solano, A.: Benzene and toluene adsorption at low concentration on activated carbon fibres. Adsorpt. J. Int. Adsorpt. Soc. **17**(3), 473–481 (2011)

Lillo-Rodenas, M.A., Fletcher, A.J., Thomas, K.M., Cazorla-Amoros, D., Linares-Solano, A.: Competitive adsorption of a benzene–toluene mixture on activated carbons at low concentration. Carbon **44**(8), 1455–1463 (2006)

Mangun, C.L., Benak, K.R., Economy, J., Foster, K.L.: Surface chemistry, pore sizes and adsorption properties of activated carbon fibers and precursors treated with ammonia. Carbon **39**(12), 1809–1820 (2001)

Mangun, C.L., Daley, M.A., Braatz, R.D., Economy, J.: Effect of pore size on adsorption of hydrocarbons in phenolic-based activated carbon fibers. Carbon **36**(1–2), 123–129 (1998)

Piccot, S.D., Watson, J.J., Jones, J.W.: A global inventory of volatile organic-compound emissions from anthropogenic sources. J. Geophys. Res. Atmos. **97**(D9), 9897–9912 (1992)

Pitzer, K.S., Scott, D.W.: The thermodynamics and molecular structure of benzene and its methyl derivatives. J. Am. Chem. Soc. **65**, 803–829 (1943)

Popescu, M., Joly, J.P., Carre, J., Danatoiu, C.: Dynamical adsorption and temperature-programmed desorption of VOCs (toluene, butyl acetate and butanol) on activated carbons. Carbon **41**(4), 739–748 (2003)

Singh, K.P., Mohan, D., Tandon, G.S., Gupta, G.S.D.: Vapor-phase adsorption of hexane and benzene on activated carbon fabric cloth: equilibria and rate studies. Ind. Eng. Chem. Res. **41**(10), 2480–2486 (2002)

Tancrede, M., Wilson, R., Zeise, L., Crouch, E.A.C.: The carcinogenic risk of some organic vapors indoors—a theoretical survey. Atmos. Environ. **21**(10), 2187–2205 (1987)

Terzyk, A.P., Gauden, P.A., Kowalczyk, P.: What kind of pore size distribution is assumed in the Dubinin–Astakhov adsorption isotherm equation? Carbon **40**(15), 2879–2886 (2002)

Wu, J.F., Stromqvist, M.E., Claesson, O., Fangmark, I.E., Hammarstrom, L.G.: A systematic approach for modelling the affinity coefficient in the Dubinin–Radushkevich equation. Carbon **40**(14), 2587–2596 (2002)